AIP | Review of Scientific Instruments

# Extending high-finesse cavity techniques to the far-infrared

Bridget Alligood DePrince, Blithe E. Rocher, Anne M. Carroll, and Susanna L. Widicus Weaver

Citation: Rev. Sci. Instrum. **84**, 075107 (2013); doi: 10.1063/1.4813274
View online: http://dx.doi.org/10.1063/1.4813274
View Table of Contents: http://rsi.aip.org/resource/1/RSINAK/v84/i7
Published by the AIP Publishing LLC.

## Additional information on Rev. Sci. Instrum.

Journal Homepage: http://rsi.aip.org
Journal Information: http://rsi.aip.org/about/about_the_journal
Top downloads: http://rsi.aip.org/features/most_downloaded
Information for Authors: http://rsi.aip.org/authors

ADVERTISEMENT


Downloaded 15 Jul 2013 to 170.140.190.145. This article is copyrighted as indicated in the abstract. Reuse of AIP content is subject to the terms at: http://rsi.aip.org/about/rights_and_permissions

# Extending high-finesse cavity techniques to the far-infrared

Bridget Alligood DePrince, Blithe E. Rocher, Anne M. Carroll,
and Susanna L. Widicus Weaver[a)]
*Department of Chemistry, Emory University, Atlanta, Georgia 30322, USA*

(Received 6 May 2013; accepted 24 June 2013; published online 15 July 2013)

Sensitive spectroscopic techniques involving high-finesse Fabry-Perot resonators are widely used in the microwave and near-infrared spectral regimes, but hardware limitations have hindered their extension to far-infrared wavelengths. While there is no theoretical limit to the frequency region where cavity-enhanced techniques are practical, the sensitivity of these methods does depend explicitly on the availability of highly reflective optics and, in the case of cavity ringdown spectroscopy, sufficiently fast detectors. Here, we describe a novel high-finesse cavity that uses wire-grid polarizers as the reflective surfaces. Quality factors on the order of $10^5$ are achieved at 250 GHz. Based on the optimized cavity design, we investigate the feasibility of extending the cavity ringdown technique to far-infrared wavelengths. With the present commercially available technology, we find spectrometer performance to be limited by both the available optics and detectors. With a 120 cm cavity and a detector response time of ~500 ns, we predict a minimum detectable absorption coefficient, $\alpha_{min}$, on the order of $10^{-7}$ cm$^{-1}$. Given the sensitivity and noise requirements for the ringdown measurements, faster and more sensitive detectors are needed before implementation of the spectrometer is practical or offers any significant advances to existing methods at far-infrared wavelengths. © *2013 AIP Publishing LLC*. [http://dx.doi.org/10.1063/1.4813274]

## I. INTRODUCTION

The terahertz (THz) frequency range, also known as the far-infrared (far-IR) region, offers access to some of the most fundamental molecular information, including low-energy vibrational modes, pure rotational transitions, and intramolecular rotation-vibration-tunneling interactions. Because internal motions guide intramolecular interactions and dictate reaction mechanisms, THz spectral studies are critical to understanding reaction dynamics. In addition to the fundamental chemical applications of THz spectroscopy, the THz frequency window overlaps with several new astronomical observatories—including the Herschel Space Observatory, the Atacama Large Millimeter/Submillimeter Array (ALMA), and the Stratospheric Observatory for Infrared Astronomy (SOFIA)—and therefore THz laboratory spectroscopy has the added opportunity to provide essential spectral information that is needed to guide observational searches for new interstellar molecules.

Despite the great deal of valuable information provided by THz spectroscopy to both the chemistry and astronomy communities, there are only a handful of high-resolution THz spectrometers in the world.[1] Most existing THz spectrometers are direct absorption instruments with limited sensitivity, restricting spectral studies to systems with relatively high concentrations of strongly absorbing, stable molecules. Even though the strongest rotational and vibrational modes of many transient molecules, such as radicals and ions, also occur in the THz range,[2] their reactive nature often dictates that they be formed and studied in low product densities to prevent further reaction. Photolysis and plasma discharge production techniques yield only trace amounts of specimen; such techniques are ideal for prohibiting further reactions with other species, but the low product yields make subsequent analysis inherently difficult. These difficulties are enhanced further by the fact that those species that do not react or dissociate are vibrationally and rotationally excited, leading to spectral complexity and weak signals. These production mechanisms can be combined with supersonic expansions to circumvent most of the aforementioned problems, but sensitivity issues still arise from small sample quantities. Therefore, the spectral characterization of highly reactive species is dependent on the development of more sensitive and selective absorption techniques in the far-IR.

Cavity-enhanced spectral techniques, relying on high-finesse Fabry-Perot resonators, are highly sensitive techniques that are often employed in the microwave and infrared regions. Indeed, the most successful studies of transient species to date have coupled supersonic expansions with high-finesse cavities, and Fourier-transform microwave (FTMW) spectroscopy[3] and cavity ringdown spectroscopy (CRDS)[4] have been the workhorses of these studies. FTMW spectroscopy has primarily been conducted at frequencies ≤50 GHz because of hardware limitations, and infrared CRDS has been limited to frequencies where lasers are available, typically >1000 cm$^{-1}$. The THz frequency range lies between these spectral windows and includes frequencies from 100 GHz to 10 THz (3–300 cm$^{-1}$). Until recently, no spectroscopic technique with sensitivities comparable to FTMW or CRDS existed for the THz range, resulting in the frequency region being described "the gap in the electromagnetic spectrum."[5] However, new developments with respect to both high-power frequency sources and sensitive heterodyne detectors have resulted in the extension of chirped-pulse

a)Author to whom correspondence should be addressed. Electronic mail: susanna.widicus.weaver@emory.edu. Telephone: +1 (0)404 7274049. Fax: +1 (0)404 7276586.

 © 2013 AIP Publishing LLC

Downloaded 15 Jul 2013 to 170.140.190.145. This article is copyrighted as indicated in the abstract. Reuse of AIP content is subject to the terms at: http://rsi.aip.org/about/rights_and_permissions

FTMW spectrometers[6] to higher frequencies.[7–9] The chirped-pulse technique provides broadband coverage of the THz range, but higher sensitivity than the minimum detectable absorption coefficient of $\alpha_{min} \sim 10^{-9}$ cm$^{-1}$ that is provided by the FTMW approach is likely needed for targeted studies of the transient species described above.

Cavity-enhanced techniques exploit the optical effects that result from the buildup of radiation within a high-finesse resonator, and they thus depend inherently on radiation coupling efficiency and on the reflectivity of the optical elements that define a particular cavity. At THz frequencies, neither the equipment nor the methodologies used in either the microwave or the infrared region are appropriate. The physical aperture used to couple radiation into the cavity in microwave applications is dominated by diffraction losses at the shorter far-IR wavelengths. Additionally, the layered dielectric mirrors commonly used in the near-IR cavity experiments are not yet available in the far-IR frequency regime.[10,11] Novel techniques must therefore be developed in order to couple radiation into and out of the cavity for THz applications. One example is given by recent experiments by Meshkov and De Lucia where a Mylar beamsplitter was used to couple radiation into and out of a 10 m cavity bound by two 12 in. diameter copper mirrors.[12] Using this design, they observed quality factors on the order of $10^6$ in the frequency range of 170–260 GHz, but the sheer scale of the spectrometer is prohibitive for many laboratories.

Another promising alternative is the use of wire-grid polarizers as both coupling elements and as the reflective, bounding surfaces. In this design, the imperfect nature of wire-grid polarizers is exploited as a means of coupling radiation into and out of the cavity. Essentially, this design manipulates the fact that ideal polarizers do not exist. An ideal polarizer is one that is completely transparent to light polarized in one direction, and completely opaque to the light polarized in the orthogonal direction. In real polarizers, however, some small component of light that should be reflected is instead transmitted. A recent report by Braakman and Blake[13] details the design of such a resonator from which they report an observed quality factor of $1.5 \times 10^5$ at frequencies around 300 GHz. This off-axis semiconfocal resonator was comprised of two wire-grid polarizers and an off-axis parabolic mirror (OAP) that served to focus the light in the cavity and maintain a stable resonator. The conclusions drawn from this study dictate fundamental limitations and design hurdles that must be considered when extending these types of high-finesse cavity techniques to the THz range. For the polarizers themselves, the optimization of the cavity quality depends upon minimizing the ratio of wire spacing to wire diameter and choosing a metal with the lowest possible resistivity. The losses incurred at the OAP could be minimized by choosing a metal with a low resistivity, minimizing the angle of incidence with respect to the incoming radiation, and increasing the focal length of the mirror. The losses at the parabolic surface, even when minimized, overwhelmingly dominated the overall roundtrip losses, and were the limiting factor in determining cavity quality.

The work described here focuses on the design and testing of three different high-finesse cavities at THz frequencies, each using wire-grid polarizers as the highly reflective, bounding surfaces. In this paper, we expand on previous findings and outline the problems inherent to these cavity designs, as well as describe an optimum cavity design and optimization process for use at THz frequencies. We also report on the magnitude of cavity losses and detector responses that can be tolerated while applying this high-finesse resonator to CRDS in the far-IR range, as well as on the lower limits for the sensitivity of the spectrometer.

## II. EXPERIMENTAL DESIGN

### A. Experimental details

The cavity designs described herein were studied using a radiation source that was comprised of an analog signal generator (Agilent Technologies, Model E8257D PSG with 1EA, UNU, 550, and UNT options), operational between 0 and 50 GHz, coupled with a Virginia Diodes amplifier and multiplier chain (Model WR10AMC) combined with two frequency triplers (Model WR-3.4 × 3); the system was capable of generating radiation in the 215–335 GHz range. Each design was tested by scanning across this frequency window, where the power output directly from the multiplier is specified to be less than 2 mW. An optical telescope consisting of two 50 cm diameter Teflon lenses (100 mm and 300 mm focal length, respectively) was used to collimate the initial beam and mode-match the beam to the cavity.

Each of the designs presented herein incorporated some combination of three different polarizers: two identical photolithographically etched gold [$\rho = 2.214 \times 10^{-8}$ Ω m at 20 °C,[14] $g = 2$ $\mu$m and $d = 1$ $\mu$m] polarizers (QMC Instruments Ltd., Mylar substrate $< 2$ $\mu$m thick, 1.5 in. diameter) and one free-standing tungsten [$\rho = 5.28 \times 10^{-8}$ Ω m at 20 °C,[14] $g = 50$ $\mu$m and $d = 20$ $\mu$m] wire-grid polarizer (Microtech Instruments, Inc. G50 × 20, 10 cm diameter). All polarizers were fixed on rotatable tilt mounts, allowing for optimization of maximum/minimum transmission grid orientations (rotation) and to better facilitate mode-matching and alignment (tilt). Three cavity configurations were tested, including two off-axis semiconfocal cavities using various combinations of the three polarizers and an off-axis parabolic mirror (OAP), and one parallel cavity using only the polarizers. For the off-axis semiconfocal cavities, a gold-coated 90° OAP with a focal length of 177.8 mm (Edmund Optics #NT63-197) was used; the mirror served to refocus and redirect the beam on each pass through the cavity, ideally minimizing any potentially incurred diffraction losses.

The radiation exiting the cavity was refocused using a 100 mm focal length Teflon lens positioned just prior to the detector. The frequency spectra shown in all figures were recorded using one of two detectors: a magnetically enhanced liquid helium cooled InSb hot electron bolometer (HEB) from QMC Instruments, Ltd. (Model QFI/2BI), or a Schottky zero-bias detector (ZBD, Model WR3.4ZBD) from Virginia Diodes, Inc.; the InSb HEB has a wide operating range (60–500 GHz), while the ZBD is specifically matched in frequency response to the multiplier chain (215–335 GHz). The detector used is specified in the additional

Downloaded 15 Jul 2013 to 170.140.190.145. This article is copyrighted as indicated in the abstract. Reuse of AIP content is subject to the terms at: http://rsi.aip.org/about/rights_and_permissions

experimental descriptions below. In all cases, a lock-in amplifier (Stanford Research Systems, Model SR830) was used to process the amplitude-modulated signal.

The tests to quantify the detector response times were implemented using two different procedures. One method used the internal pulse generator (UNU option) on the Agilent frequency synthesizer to modulate the RF amplitude. An additional method was also tested, whereby a digital delay generator (Stanford Research Systems, Model DG645) was used to apply a 0–5 V DC TTL pulse directly to a TTL-modulation BNC input on the multiplier chain, resulting in signal oscillation between full power and no power out, respectively. Both methods yield identical results but were performed in sequence to rule out the possibility of delays inherent to a specific triggering method.

One test utilized an aluminum 15° off-axis parabolic mirror (Edmund Optics NT69-159), as it is commercially available from Edmund Optics with longer focal lengths than the 90° OAP. $TEM_{00}$ mode structures were not observed using this setup; this is likely due to difficulties with mode-matching upon reflection at the curved surface.

## B. Experimental considerations: Expected cavity losses and theoretical limits

The quality of a cavity is defined by its quality factor, $Q$, which describes the ratio of stored power to rate of power dissipation. The $1/e$ ringdown time, $\tau$, is directly proportional to the cavity quality and, in the specific case of the off-axis semiconfocal cavities described here,[13] is inversely proportional to $\alpha_{RT}$, the roundtrip loss per pass of the cavity. In the limit where the reflectivity, $R$, approaches unity, the following relationship is valid:

$$\tau = \frac{Q\lambda}{2\pi c} = \frac{2L}{\alpha_{RT} c}. \tag{1}$$

Here, $\lambda$ and $c$ are the wavelength and speed of light, respectively; $\alpha_{RT}$ combines both inherent losses due to imperfections in the cavity and losses due to the presence of an absorbing species, and $L$ is the overall length of the cavity, e.g., twice the focal length of the OAP being used.

From Eq. (1), it is clear that there are two obvious choices to increase the cavity quality and thus also the ringdown time: the cavity length can simply be increased, or, with perhaps a bit more effort, the roundtrip losses can be further decreased. Braakman and Blake[13] present detailed equations that quantify expected losses from these types of cavities: given the surfaces with which the radiation interacts (i.e., wire-grid polarizers or parabolic mirrors) the predicted loss factors can be calculated. The anticipated losses for our specific cavity design are detailed in Secs. II B 1 and II B 2. We note here that diffraction losses are taken to be negligible, unless otherwise noted.

### 1. Expected losses upon reflection at the wire-grid polarizers

To minimize reflective losses at the wire-grid bounding surfaces, three physical characteristics of the wire grid must be considered: the resistivity of the metal wires, the diameter of the metal wires, and the period of the wire grid. We use the same fundamental equations given by Braakman and Blake[13] to quantify the losses anticipated upon reflection at each polarizer. However, a detailed check of the equations given in this reference reveal a typographical error in the equation for the effective loss resistance [Eq. (11) in Ref. 13]; the error was carried through to the final reflectivity expression [Eq. (15) in Ref. 13] and the total losses incurred at one pass of a wire-grid polarizer [Eq. (17) in Ref. 13]. The correct expression for the effective loss resistance, $R_l$, is given by

$$R_l = R_s \frac{2g}{u} = \sqrt{\frac{4g^2 Z_0 \rho}{\pi d^2 \lambda}}, \tag{2}$$

which is larger by a factor of $(2g/d)^{1/2}$ than the equation given by Braakman and Blake.[13] Here, $R_s$ and $\rho$ are the surface resistance and resistivity of the metal comprising the wire grid, respectively; $g$ is the wire spacing, $u$ is the wire circumference, $d$ is the wire diameter, and $Z_0$ is the impedance of free space ($Z_0 = \mu_0 c \sim 376.73\ \Omega$ m). The corrected corresponding expressions for the reflectivity of the grid (Eq. (3)) and the total loss of the grid, $\alpha_{wg,free\text{-}standing}$ (Eq. (4)) are

$$\mathbf{R} = \frac{1}{\left((1+\sqrt{\frac{16g^2\rho}{\pi d^2 Z_0 \lambda}})\right)^2 + \left(\frac{\lambda \ln\left(2g^2/d^2 - 1 + (2g/d)\sqrt{g^2/d^2 - 1}\right)}{2\pi^2 l}\right)^2}, \tag{3}$$

$$\alpha_{wg,free\text{-}standing} = 8\sqrt{\frac{4g^2\rho}{Z_0 \pi d^2 \lambda}}. \tag{4}$$

The parameter $l$ introduced in Eq. (3) describes the length of the wires. We note here that the anticipated losses are calculated for the free-standing wire-grid polarizers used by Braakman and Blake, consisting of a fine array of tightly wound tungsten wires. For some of the designs presented in the current work, an identical polarizer to the free-standing polarizer used by Braakman and Blake has been used, and the above equations hold.

Downloaded 15 Jul 2013 to 170.140.190.145. This article is copyrighted as indicated in the abstract. Reuse of AIP content is subject to the terms at: http://rsi.aip.org/about/rights_and_permissions

For reasons of mechanical integrity, however, photolithographically etched polarizers are often preferable. Additionally, lithographic manufacturing techniques are capable of engineering higher pitch metallic grids, and thus these grids have the added benefit of greater efficiency at higher frequencies than the free-standing wire-grid counterpart.[15,16] These etched polarizers consist of a pattern of thin parallel strips of metal deposited on the surface of an ultrathin polymer substrate; in the current work, polarizers consisting of gold strips etched into a Mylar substrate (<2 $\mu$m thickness, per manufacturer specifications) have been used. For the etched polarizers, minor modifications to the above equations must be incorporated to account for different wire geometries. Because of the methods with which the wires are deposited onto the Mylar substrate thin films, their physical shape is more like a rectangular "strip" than a cylindrical wire. The change in shape effectively alters the $2g/u$ multiplication factor, introduced in Eq. (2) to account for the grid-like nature of the metal, to a factor of $g/d$.[13,17] The resulting loss equation for the etched polarizers is thus

$$\alpha_{wg,etched} = 8\sqrt{\frac{g^2\rho\pi}{Z_0 d^2 \lambda}}. \tag{5}$$

An added potential complication that is introduced through the use of the etched polarizers is reflection off of the Mylar substrate. This complication is a small one given the ultrathin nature of the film. However, unlike with the free-standing wire-grid polarizers, it is now possible to get imperfect transmission of the component of light perpendicular to the conducting wires, as that light could inadvertently be reflected off of the substrate surface. To minimize any observable effects from imperfect transmission, we use the photolithographically etched polarizers as the bounding surfaces.

#### 2. Expected losses upon reflection at the OAP

We use the expression given by Braakman and Blake,[13] derived from and equivalent to that contained in Ref. 13, to predict the losses incurred upon reflection at the 90° OAP:

$$\alpha_{OAP} = \alpha_c + \alpha_{ba} = 4\sqrt{\frac{2\pi\rho}{Z_0\lambda}} + \frac{3\lambda}{4\pi F}. \tag{6}$$

Here, $F$ and $\rho$ are the focal length and resistivity of the OAP substrate, respectively, and all other terms are equivalent to the parameters defined in Sec. II B 1. In this expression, $\alpha_c$ accounts for conductance loss at the metal surface and $\alpha_{ba}$ incorporates losses due to both beam-distortion and cross-polarization of the beam; both terms are simplified versions of the more generic equations given in Refs. 13 and 18 and are thus applicable only to the off-axis semiconfocal 90° arrangement such as that presented herein.

#### 3. Detector sensitivity and responsivity requirements

Cavity ringdown spectroscopy operates on the principle that the rate of decay of the intensity of light in the cavity is inherently related to the losses incurred during roundtrip passes through the cavity; the losses are the sum of both inherent cavity losses and absorption by molecular species present in the cavity. The success of CRDS in any frequency regime therefore fundamentally depends on the ability to fit a given decay curve to the aforementioned loss parameters. For a molecular species with a very small absorption coefficient, the fitting is extremely dependent both on the noise present in the detected curve and the response time of the detector.

To get a quantitative understanding of the types of noise and detector responses that could be tolerated before losing quantitative information from the spectrometer, one must consider the difference in the parameter that will be measured, with and without an absorbing species present. Equation (1) gives the relationship between the ringdown time, $\tau$, and the round-trip losses, $\alpha_{RT}$. Consider explicitly how the roundtrip losses are incurred:

$$\alpha_{RT} = \alpha_{empty} + \alpha_{absorber} \times b, \tag{7}$$

where $\alpha_{empty}$ is the summed empty-cavity loss described in Secs. II B 1 and II B 2, i.e., from reflection or diffraction, and $\alpha_{absorber}$ is the absorption coefficient (units of $cm^{-1}$) of any absorbing molecular species present over a path length $b$ within the cavity; it is the latter quantity that will be measured. The sensitivity with which the absorption coefficient can be quantified is therefore completely dependent on the accuracy and precision with which the ringdown curves can be measured and fit. By substituting Eq. (7), the expanded term for round-trip losses, into Eq. (1), the relationship between an empty cavity (i.e., $\alpha_{absorber} = 0$) and a cavity in which an absorbing molecular species is present (i.e., $\alpha_{absorber} \neq 0$) can be defined as follows:

$$\tau_{empty} - \tau_{sample} = c \times \alpha_{absorber} \times \tau_{empty} \times \tau_{sample}. \tag{8}$$

For simplicity, Eq. (8) applies to the generic case where the sample occupies the entire cavity. It is important to note that in cases where cavity-enhanced techniques are coupled to supersonic expansions, the path length of light through the sample is considerably shorter. Rearranging Eq. (8) to solve for $\alpha_{absorber}$, the quantity to be measured, yields

$$\alpha_{absorber} = \frac{1}{c}\left(\frac{1}{\tau_{sample}} - \frac{1}{\tau_{empty}}\right). \tag{9}$$

For the limiting case where the error in $\tau_{sample}$ is the same as $\tau_{empty}$, the change in $\alpha_{absorber}$, $\partial\alpha_{absorber}$, is directly dependent on the change in $\tau_{empty}$, $\partial\tau_{empty}$, by the following relationship:

$$\partial\alpha_{absorber} = \frac{\sqrt{2}}{c\tau_{empty}^2}\partial\tau_{empty}. \tag{10}$$

By minimizing the detectable change in $\partial\tau_{empty}$, the minimum detectable $\partial\alpha_{absorber}$ can be directly influenced. The limit to which $\partial\tau_{empty}$ can be effectively minimized is outlined in Sec. III.

## III. EXPERIMENTAL RESULTS

Three different cavity designs were tested. The results from the three trials are summarized in Table I. The specific

Downloaded 15 Jul 2013 to 170.140.190.145. This article is copyrighted as indicated in the abstract. Reuse of AIP content is subject to the terms at: http://rsi.aip.org/about/rights_and_permissions

TABLE I. Summary of the various cavity designs, their considerations and limitations, described herein.

| | Summary |
|---|---|
| Scheme 1a: Detector Position 1 | Difficulties with mode-matching and alignment due to overwhelming background signal at the detector. |
| Scheme 1b: Detector Position 2 | Proximity to the source makes alignment of detector difficult. Spatial constraints for detector positioning. Loss of power from introduction of beamsplitter to detection scheme. |
| Scheme 2 | Lack of intracavity focusing element causes diffraction losses to dominate. |
| Scheme 3 | Diffraction losses are minimized through addition of OAP. Background signal at the detector is minimized by using a third polarizer, sandwiched between the two polarizers used in Scheme 1, as a filter. |

details of each cavity arrangement and the corresponding results are given below.

### A. Scheme 1: 2-polarizer off-axis semiconfocal cavity

To begin our studies, we attempted to replicate the off-axis semiconfocal cavity presented by Braakman and Blake.[13] This design, a schematic of which is shown in Fig. 1, uses the two photolithographically etched polarizers, with identically oriented grids, to both couple and trap the radiation; a 90° OAP is used to focus the radiation internally upon successive passes of the cavity. The polarizers are placed at a distance corresponding to the focal length of the OAP. Most of the light that passes through the first polarizer has polarization perpendicular to the wires; the now linearly polarized light will be transmitted through the second polarizer as well, as the polarizers are identically oriented, and thus will not constitute the "ringing" signal trapped in the cavity. However, because no polarizer is perfect, there is a small fraction of the incident radiation that is transmitted ("leaked") through the first

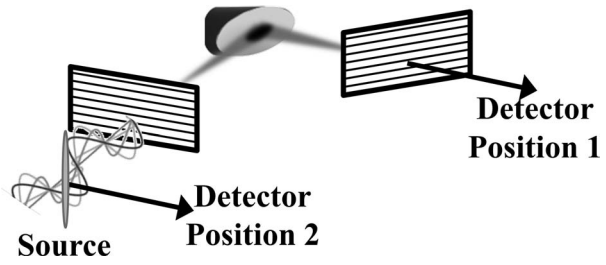


FIG. 1. Schematic of basic off-axis semiconfocal resonator used by Braakman and Blake.[13] and replicated in the present work. Here, the input and output polarizers are positioned at a distance corresponding to the focal length of the 90° OAP and serve to both couple and trap the radiation within the cavity. The imperfect nature of the polarizer allows a small component of light with its electric field oriented parallel to the conducting wires into the cavity; this light gets trapped between the two identically oriented polarizers. The OAP serves to refocus the beam upon successive passes, thus minimizing diffraction losses due to divergence. When detecting at Position 1, background signal overwhelms the cavity mode structures. Background can be avoided by detecting at Position 2, but its proximity to the source makes alignment (and hence mode-matching) prohibitively difficult.

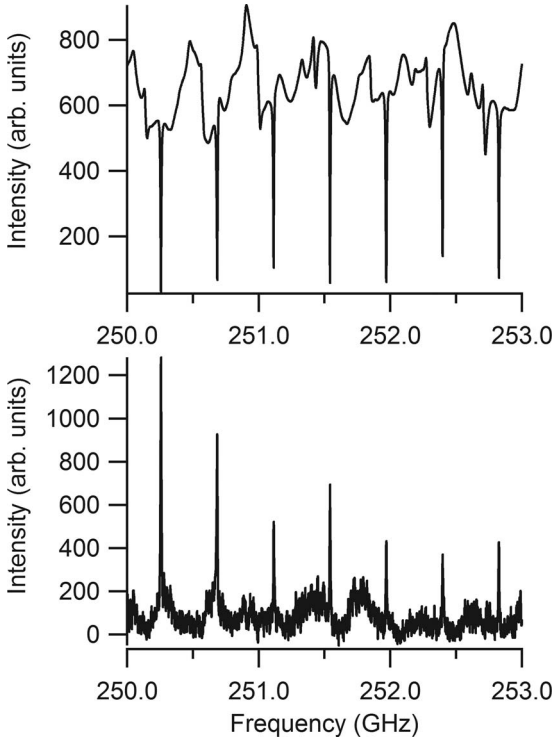


FIG. 2. Typical frequency response of an off-axis semiconfocal cavity arrangement as shown in Fig. 1 (similar to that in Ref. 13). The upper frame shows signal observed by detecting at Position 1 with the HEB, and the lower frame shows signal observed detecting at Position 2 with the ZBD. The observed free spectral range of the resonator is 421 MHz, which corresponds to a cavity length of approximately 36 cm, equal to the separation between the polarizers. The negative-pointing "mode shadows" shown in the upper frame are due to destructive interference of the "ringing" signal with the background signal. The background signal can be filtered by detecting light reflected off of a beamsplitter at Position 2. Positive mode structures are then observed, e.g., build-up of signal as the cavity is tuned to a resonant frequency, but the proximity of the detector to the initial source radiation makes alignment and mode-matching prohibitively difficult.

polarizer with its electric field parallel to the wires; it is this signal that consequently gets trapped between the two polarizers and leads to the cavity mode signals. It should be noted that the degree of polarization at the source, e.g., the purity of the source, would only affect the relative intensity of both the background transmission and the cavity mode signals. Because it is the "non-pure" component of the source that gets coupled into the cavity, the fraction of light that comprises the cavity mode signals versus the background signal is directly dependent on the initial polarization of the source.

Typical frequency spectra obtained with the off-axis semiconfocal cavity are shown in Fig. 2. The spectrum shown in the upper frame was taken using the InSb HEB detector, but the spectrum in the lower frame required that the more compact ZBD be used because of spatial constraints. The observed free spectral range of the cavity is 421 MHz, corresponding to a cavity length of approximately 36 cm, roughly double the focal length of the OAP. It should be noted that the results given by Braakman and Blake[13] showing positive mode structures (e.g., corresponding to an increase in signal upon tuning to a resonant frequency) could not be reproduced. Instead, it was found that background signal, e.g., the signal resulting from light with a polarization perpendicular

Downloaded 15 Jul 2013 to 170.140.190.145. This article is copyrighted as indicated in the abstract. Reuse of AIP content is subject to the terms at: http://rsi.aip.org/about/rights_and_permissions

to the wires and thus directly transmitted through both grids, dominated the detector response when the detector was placed immediately after the second polarizer (Position 1 in Fig. 1); the signal arising from tuning to a resonant frequency of the cavity is complicated by the background, and the modes appear as a loss in signal, rather than an increase (upper frame of Fig. 2). We term the observed structures "mode shadows," as they result from destructive interference with the background signal at on-resonance frequencies. To test that background signal was indeed the culprit, a Mylar beamsplitter was introduced before the cavity, and the reflected signal was recorded (Position 2 in Fig. 1). A representative spectrum is shown in the lower frame of Fig. 2 and shows that the background signal was effectively eliminated. However, in this configuration, the proximity of the detector to the initial source made alignment and mode-matching issues challenging; it is because of these challenges that quantitative conclusions regarding cavity quality could not be drawn. Additionally, the introduction of the beamsplitter results in a non-negligible loss of power from observed mode structures and would negatively impact the signal level, and thus fitting procedures, associated with detection of observed mode structures.

### B. Scheme 2: Proof-of-concept linear cavity

To address the issue of background signal, a third polarizer was added between the two photolithographically etched polarizers used in Scheme 1. The polarizer had an orthogonal orientation relative to the other two polarizers; for simplicity in the proof-of-concept test, the OAP was removed. The free-standing tungsten grid was chosen as the middle polarizer in an effort to eliminate any contributions to round-trip losses incurred via absorption by the Mylar substrate present in the photolithographically etched polarizers. Absorption losses should be negligible,[19] but by using the free-standing wire-grid polarizer, they were avoided entirely.

In this configuration, most of the light that passes through the first polarizer will be reflected off of the second polarizer, back toward the source. Only a small cross-polarized component will be transmitted through the second polarizer. In this way, the second polarizer is introduced essentially to purify the signal, eliminating background signal at the detector. Although adding this polarizer before the initial polarizer would, in theory, serve the same purpose, the overall signal-to-noise ratio of the detected cavity mode signals would be greatly reduced. Because a polarizer transmits a certain percentage of the light that impinges upon it, adding this polarizer outside of the cavity would essentially result in lower intensity cavity modes, and thus a spectrometer with lower sensitivity. For these reasons, especially given the low power of the source and the sensitivity of the detector, we chose to add the polarizer in the middle of the cavity where these effects are minimized. Figure 3 shows a proof-of-concept design illustrating how the three polarizers in succession serve to couple and trap the incoming radiation. Typical mode structures observed with this configuration are shown in Fig. 4 and display a free spectral range of approximately 1.2 GHz, corresponding to the spacing of the front and back polarizers of

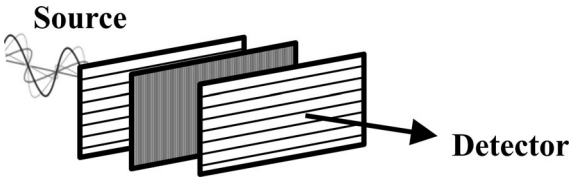


FIG. 3. Schematic of the linear cavity used as proof-of-concept in the current work. Here the middle polarizer is oriented with its wires 90° to the front and back polarizers; the orthogonal position serves to purify the polarization of the intracavity signal and eliminates background signal at the detector.

12.5 cm; the spectrum was recorded using the InSb HEB. Without an intracavity focusing element, diffraction dominates the overall round-trip losses; as the radiation completes multiple passes through the cavity, imperfections in initial collimation are amplified. Therefore, in an effort to minimize the overall path length and thus the magnitude of beam divergence, the polarizers were placed as close together as was possible (total separation of 12.5 cm), limited by the optics mounts. As indicated by the large observed FWHM of 80 MHz, which corresponds to a cavity quality $Q$ of $3.13 \times 10^3$, the linear cavity design suffers from overwhelming diffraction losses.

### C. Scheme 3: 3-polarizer off-axis semiconfocal cavity

To avoid the issues presented in Subsections III A and III B, i.e., detector alignment and background signal, we combined critical elements from the previous two design schemes. This design uses a third polarizer to eliminate background signal at the detector, combined with an intracavity focusing element to minimize diffraction losses; a schematic of the design is given in Fig. 5. Two photolithographically etched grid polarizers were placed at a distance from the OAP corresponding to its focal length. A third polarizer, the free-standing tungsten grid, was placed at an arbitrary position between the front polarizer and the OAP. The middle polarizer was tilted slightly with respect to the front polarizer, ensuring that the two were not perfectly parallel. The observed mode structures with a tilted middle polarizer were more uniform

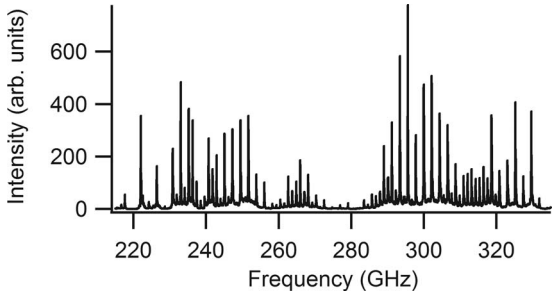


FIG. 4. Typical frequency spectrum observed with a linear cavity using three polarizers in succession (seen in Fig. 3). The free spectral range of the cavity is approximately 1.2 GHz, which is in agreement with the spacing of ~12.5 cm between the first and last polarizers. The spectrum is riddled with higher order $TEM_{mn}$ modes as well as a rolling baseline from etalons. Diffraction losses dominate (FWHM ~ 80 MHz, $Q = 3.13 \times 10^3$) and are unavoidable due to imperfections in the initial beam collimation and the lack of an intracavity focusing element.

Downloaded 15 Jul 2013 to 170.140.190.145. This article is copyrighted as indicated in the abstract. Reuse of AIP content is subject to the terms at: http://rsi.aip.org/about/rights_and_permissions

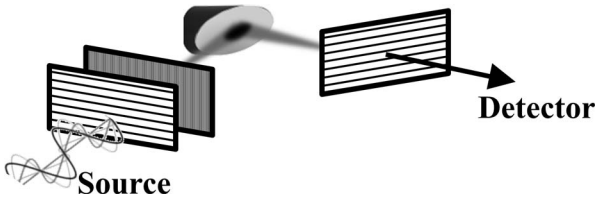


FIG. 5. Schematic of the final optimized design that uses critical components from the previous two designs to address the issues of background signal, diffraction losses, and detector alignment efficiency. Here, the front and back polarizer, with wires identically oriented, are placed at a distance from the OAP corresponding to the focal length of the mirror; these two polarizers serve as the bounding surfaces of the cavity. The middle polarizer is placed at an arbitrary distance between the front polarizer and the OAP. In this design, the first polarizer is used to transmit a small portion of the light with its electric field oriented parallel to the conducting wires. This light is transmitted through the second polarizer and trapped between the front and back polarizers. The majority of the light that is transmitted through the first polarizer is reflected off of the middle polarizer, thus eliminating the presence of dominant background signal at the detector. The OAP is used, in a fashion similar to Scheme 1, to focus and refocus the beam upon successive passes through the cavity.

with respect to peak power than in the case without tilting the middle polarizer. It is unclear whether tilting the middle polarizer served to eliminate standing waves between the middle polarizer and another optical component, or whether tilting the polarizer effectively minimized the clear aperture to a point where it blocked higher order modes with nodes that did not fall in the aperture of the polarizer. A typical frequency spectrum, obtained with the HEB, is given in Fig. 6. The free spectral range of the cavity is equivalent to the design shown in Fig. 1, confirming that the overall cavity length is undisturbed by adding a middle polarizer; the two photolithographically etched polarizers constitute the bounding surfaces for the high-reflectivity cavity.

The result of the optimized cavity design is a much cleaner mode spectrum, owing to the ease of mode-matching and alignment and the removal of background signal. Therefore, quantitative cavity parameters can be extracted. Assuming that diffraction losses are negligible, and likewise that absorption of the Mylar sheet on which the photolithographically etched polarizers are mounted is negligible,[19] we can

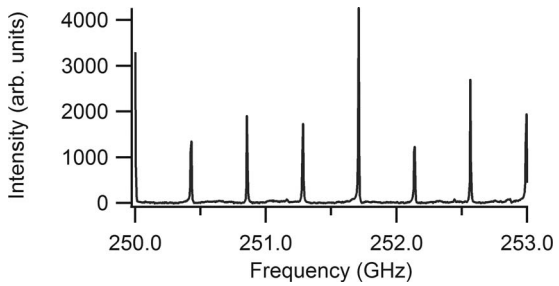


FIG. 6. Typical frequency spectrum observed with an off-axis semiconfocal cavity arrangement using three polarizers (seen in Fig. 5). The free spectral range of the cavity is identical to the design shown in Fig. 1, confirming that the two outermost polarizers are forming the bounding surface; the middle polarizer does not affect the cavity other than to eliminate the presence of background signal at the detector. The narrowest observed $TEM_{00}$ modes have a FWHM of approximately 2 MHz in this frequency region, corresponding to a measured $Q$ of $1.25 \times 10^5$, close to the theoretical value of $1.85 \times 10^5$.

calculate from Eqs. (5) and (6) the anticipated losses incurred:

$$\alpha_{RT} = \alpha_{empty} = 2 \times \alpha_{wg,etched} + 2 \times \alpha_{OAP} = 2 \times 6.3 \times 10^{-3} + 2 \times 3.82 \times 10^{-3} = 2.02 \times 10^{-2}. \quad (11)$$

The calculated loss corresponds to a reflectivity, $R = (1 - \alpha_{RT})^{1/2}$, of 98.99% and an anticipated quality factor, $Q$, of $1.85 \times 10^5$. From the full-width-at-half maximum (FWHM) of the observed mode structures, the corresponding observed quality factor can be derived from the relationship $Q = \nu \times (\mathrm{FWHM})^{-1}$; here, $\nu$ is the frequency of the detected light. The observed modes had a FWHM of 2 MHz, corresponding to a $Q$ of $1.25 \times 10^5$ at 250 GHz. Thus, the observed losses match the limit of the theoretical polarizer/OAP losses calculated in Eq. (11) to within ~70%.

### D. Hardware limitations

There is a delicate balance involved with selecting an appropriate quality factor for a given Fabry-Perot resonator because it directly impacts the ringdown time. A cavity with too high of a quality factor can limit data acquisition rates: the longer the ringdown event, the longer the required acquisition time. Higher quality factors and reflectivity also result in less power reaching the detector, thus negatively impacting signal-to-noise and fitting accuracy. In a similar way, and more pertinent to the studies contained herein, a value of $Q$ that is too small and corresponds to a ringdown event shorter than the detector rise/fall time is not experimentally useful.[20] Thus, the required magnitude of the ringdown time depends on the response time of the detector and the noise at the detector; the detector must have a sufficiently short response time to enable detection of enough of the ringdown event that the fitting parameter is not significantly affected. We describe in Secs. III D 1 and III D 2 the hardware limitations pertaining to both increasing the cavity length, and thus the length of the decay curve and ringdown time, and minimizing the response time of the detector.

#### 1. Ringdown time limits (cavity lengths)

One obvious solution to increasing the ringdown time is to lengthen the cavity. This would require a longer focal length OAP and either better collimation of the initial beam or a larger radius optic so as to maintain minimal diffraction losses. Custom-made off-axis parabolic mirrors are available commercially with a wide range of focal lengths, diameters and substrate/coating options. Figure 7 shows the decay curves that would be expected using the same three polarizers from Sec. III C, but adjusting the focal length and diameter of the gold 90° OAP (and thus the length of the overall cavity); by increasing the diameter with the focal length, diffraction losses can again be assumed to be negligible. The curves clearly demonstrate the benefit of increasing the cavity length, specifically as it concerns the effect introduced by the detector response. Table II contains similar information, but includes more parameters associated with the cavity quality. Because

Downloaded 15 Jul 2013 to 170.140.190.145. This article is copyrighted as indicated in the abstract. Reuse of AIP content is subject to the terms at: http://rsi.aip.org/about/rights_and_permissions

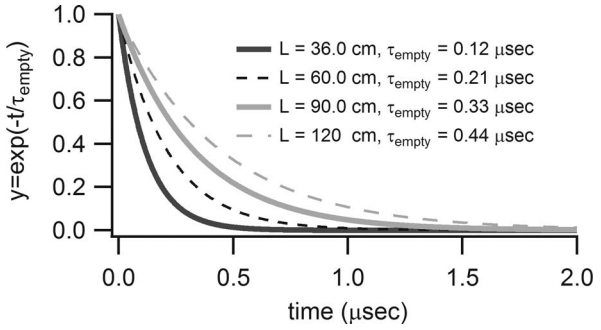


FIG. 7. Anticipated decay curves for various empty cavities (i.e., with no absorber present) of differing lengths. The empty-cavity decay rate, $\tau_{empty}$, is defined as the time it takes the signal to decay to $1/e$ of its initial value. The decay rate is inversely proportional to $\alpha_{empty}$ and directly proportional to $L$. While $\alpha_{empty}$ can be minimized by judicious choice of metal and polarizer designs, there are fundamental hardware limitations that dictate the lower limits to the losses. Once these limitations are met, the only way to increase $\tau_{empty}$ is to increase the focal length of the OAP, effectively minimizing $\alpha_{OAP}$ and maximizing the cavity length, $L$.

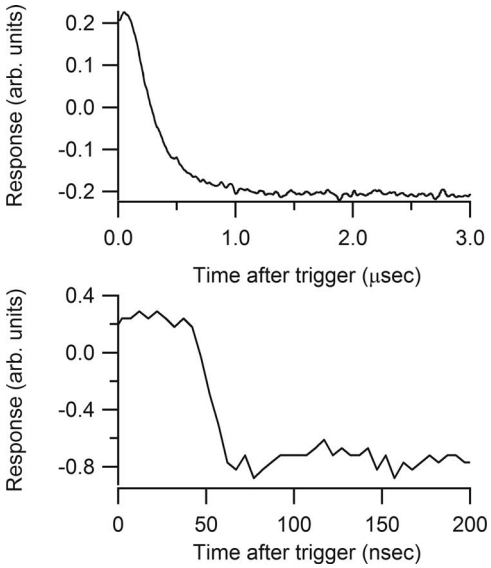


FIG. 8. Observed response time using the InSb hot electron bolometer (upper frame) and zero bias diode detector (bottom frame). The response time of the ZBD is at least an order of magnitude faster than that of the HEB, but the signal-to-noise is noticeably lower. Both response time and sensitivity must be taken into account when choosing a detector for CRDS experiments.

we seek to avoid the prohibitively large-scale size of the cavity outlined by Meshkov and De Lucia,[12] we extend the length out to a manageable 120 cm, corresponding to the longest focal length OAP (60 cm) that was quoted from commercial manufacturers.

### 2. Detector response and sensitivity limitations

Figure 8 reveals the measured response times of the two detectors that were used for these measurements. The upper frame shows the response of the InSb HEB with respect to the frequency source being triggered off. Similarly, the bottom frame shows the same response when observing the signal with the ZBD. The HEB exhibits a $1/e$ response of ~500 ns. Although we did try reducing the response time even further by removing the magnets from the detector block, we note that the response is ultimately dominated by the electron-phonon relaxation time of ~300 ns in InSb at 4.2 K.[21] Thus, the effect of removing the magnets is likely to be minimal, and indeed we observed no noticeable change in the response time with their absence. The ZBD is obviously much faster to respond, with a response time on the order of a few tens of nanoseconds, but the signal-to-noise of the resultant spectrum is markedly worse.

To quantify the anticipated detectable $\alpha_{absorber}$ feasible with the HEB response time, we generated 100 generic ringdown curves exhibiting a ringdown time $\tau_{empty}$ as calculated from the theoretical cavity losses (Table II). Figure 9 shows one such curve, designed to mimic the signal expected from an optimized 120 cm length cavity; a random number generator was used to simulate noise, yielding a reasonable signal-to-noise ratio of $10^2$. The 100 generated curves were then fit at varying degrees of truncation to mimic the effects of the non-zero detector response times. The fitting procedure was based on that given by Halmer *et al.*[22] The standard deviation of the 100 fitted $\tau_{empty}$ values was set as the lower limit for the minimum detectable change in $\tau_{empty}$, $\partial\tau_{empty,min}$. According to Eq. (10), $\partial\tau_{empty,min}$ corresponds directly to the minimum detectable absorption coefficient of an absorber, $\partial\alpha_{absorber,min}$. Using the calculated standard deviation, we can therefore predict the sensitivity of our spectrometer; the results of the fitting procedures are given in Table III. As a best-case scenario, this spectrometer is only sensitive to species with an absorption coefficient, $\alpha_{absorber}$, greater than roughly $10^{-7}$ cm$^{-1}$. It should be stressed that these calculations give the absolute lower limits to detection sensitivity. Therefore, the spectrometer does not offer significant improvement over existing direct absorption measurements, which routinely achieve $\alpha_{min}$ values of $\leq 10^{-7}$ cm$^{-1}$, and multipass optical arrangements that have been shown to achieve $\alpha_{min} \geq 10^{-9}$ cm$^{-1}$.[23]

TABLE II. Parameters describing the cavity quality that is theoretically achievable using the current set of polarizers, arranged as shown in Fig. 5. The only difference between the scenarios is the focal length of the (gold) OAP. In each case, the total cavity length $L$ is achieved by the addition of an OAP with focal length $F = L/2$, and placing the polarizers at an approximate distance F on each side of the OAP. In all cases, diffraction losses are assumed to be negligible.

| L (cm) | R | $\tau$ ($\mu$s) | Q | Finesse | FSR (MHz) | FWHM (MHz) | $L_{eff}$ (cm) |
|---|---|---|---|---|---|---|---|
| 36 | 0.9899 | 0.1181 | $1.854 \times 10^5$ | 308.9 | 416.4 | 1.348 | 3539 |
| 60 | 0.9905 | 0.2102 | $3.301 \times 10^5$ | 329.9 | 249.8 | 0.757 | 6301 |
| 90 | 0.9908 | 0.3264 | $5.126 \times 10^5$ | 341.5 | 166.6 | 0.488 | 9785 |
| 120 | 0.9910 | 0.4430 | $6.958 \times 10^5$ | 347.7 | 124.9 | 0.359 | 13280 |

Downloaded 15 Jul 2013 to 170.140.190.145. This article is copyrighted as indicated in the abstract. Reuse of AIP content is subject to the terms at: http://rsi.aip.org/about/rights_and_permissions

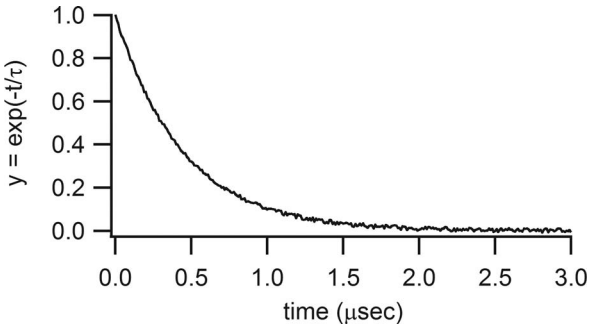


FIG. 9. Simulated ringdown curve for a theoretical cavity with a length of 120 cm. The curve includes anticipated noise levels and is typical of the 100 curves generated and fit to yield the parameters shown in Table III.

## IV. DISCUSSION

As shown above, recent technical advances have made feasible the design of high-finesse Fabry-Perot resonators for the THz range and bring promise for advancing spectral capabilities in the "THz gap." The extension of highly sensitive cavity-enhanced techniques into the THz frequency region would allow for the study of transient species that have historically eluded characterization at far-IR wavelengths.

We describe here an optimized THz Fabry-Perot cavity that uses wire-grid polarizers as reflective surfaces. The design uses three polarizers to minimize background signal at the detector and to maximize alignment efficiency, and an intracavity focusing optic to minimize diffraction losses upon successive passes through the cavity. Our results present a discrepancy with Braakman and Blake.[13] Unlike their reported results, using just two polarizers as bounding surfaces, we find that background dominates and observe "mode shadows" rather than positive mode structures. By adding a middle polarizer, with the grid having an orthogonal orientation to the front and back polarizers, the background signal can be effectively filtered out and both mode-matching and detector alignment efficiency can be enhanced.

The optimized scheme described herein is ultimately designed to minimize losses per pass, effectively maximizing the ringdown time. The biggest factors influencing cavity quality, and thus the ringdown time, are the length of the cavity and the material comprising the reflective surfaces, in particular the resistivity of the metal. While choosing a metal with lower resistivity is beneficial and will increase the cavity quality, the gains introduced are not of the order of magnitude needed to make a substantial difference. As an example, copper has a resistivity of $1.68 \times 10^{-8}$ Ω m at 20 °C.[14] Let us consider the 120 cm cavity: if we were to instead use wire-grid polarizers made out of copper strips, as compared to the gold ($\rho = 2.2 \times 10^{-8}$ Ω m at 20 °C[14]) polarizers used here, we would effectively increase the ringdown time to 490 ns – not substantially higher than the 447 ns predicted from our current design parameters (see Table II or Figs. 7 and 9). Because the effect of a better-quality wire grid is negligible compared with the added benefit of a longer cavity, we have not invested in newer and better polarizers at this stage in the instrument development.

We note that the detector response and sensitivity are the limiting factors, ultimately determining the overall sensitivity of the spectrometer. An OAP with a focal length of 60 cm, corresponding to an overall cavity length of 120 cm, is at the limit of current commercial manufacturing capabilities. As shown in Table II, a 120 cm cavity is expected to exhibit a theoretical ringdown time of approximately 440 ns, which is almost identical to the observed detector response time. Within these limits, and considering a best-case scenario, the minimum detectable absorption coefficient, $\alpha_{absorber}$, that could be measured with this cavity is on the order of $10^{-7}$ cm$^{-1}$, two orders of magnitude less than increased-path length direct absorption techniques[23] or chirped-pulse FTMW techniques.[7] The construction of a cavity ringdown spectrometer at THz frequencies does not offer any added benefits to existing technology, and it thus awaits the development of a faster and more sensitive detector.

TABLE III. Fitting parameters obtained from fitting a series of 100 simulated ringdown curves, such as that shown in Figure 9, at various points of truncation. The curves were generated in order to approximate the sensitivity achievable with a system composed of a 60 cm focal length OAP (i.e., 120 cm cavity). The signal-to-noise ratio was approximated to $10^2$.

| Truncation (ns) | Average $\tau$ ($\mu$s) | St. dev. ($\tau$) (ns) | $\partial\alpha_{\min}$ (cm$^{-1}$) |
|---|---|---|---|
| 0 | 0.4428 | 0.933 | $2.244 \times 10^{-7}$ |
| 200 | 0.4429 | 1.466 | $3.526 \times 10^{-7}$ |
| 400 | 0.4427 | 2.232 | $5.368 \times 10^{-7}$ |
| 600 | 0.4428 | 3.199 | $7.693 \times 10^{-7}$ |
| 800 | 0.4432 | 5.578 | $1.344 \times 10^{-6}$ |
| 1000 | 0.4431 | 8.485 | $1.471 \times 10^{-6}$ |

## V. CONCLUSION

Wire-grid polarizers function as highly reflective surfaces in the THz frequency range and offer the promise of extending high-finesse cavity techniques to the far-infrared. Here, we describe the development of one such cavity that uses wire-grid polarizers as both the coupling elements and bounding, reflective surfaces. Quality factors on the order of $10^5$ were achieved for an input frequency of 250 GHz. From the design performance, we investigated the feasibility of extending the cavity ringdown technique to THz frequencies, where more sensitive spectroscopic techniques are required. The extension of CRDS to the far-IR would allow for the spectral characterization of reactive, transient species in the gas phase and would offer valuable information to both the chemistry and astronomy communities. However, with current commercially available technology, we find spectrometer performance to be limited by both the available optics and detectors. While ringdown events can be lengthened to overcome detector response times by using an OAP of a longer focal length, the manufacturing cost and size of the resulting instrument would be prohibitive for many laboratories. Therefore, given the sensitivity and noise requirements for ringdown measurements, detectors with increased response times and sensitivities are needed before implementation of the spectrometer is practical or offers any significant advantages to methods that currently exist at far-IR wavelengths.

Downloaded 15 Jul 2013 to 170.140.190.145. This article is copyrighted as indicated in the abstract. Reuse of AIP content is subject to the terms at: http://rsi.aip.org/about/rights_and_permissions

## ACKNOWLEDGMENTS

The authors thank Geoffrey Blake for the loan of the tungsten polarizers, and Ken Wood and QMC Instruments, Ltd. for the photolithographically etched gold polarizers. The authors acknowledge Brandon Carroll and Brett McGuire for initial construction of cavity scheme 1. The authors also thank Emory University for the facilities and staff support that enabled this work. This work was funded in part by NASA award NNX11AI07G, NSF award CHE-1150492, and SLWW's startup funds from Emory University.

[1]M. Tonouchi, Nat. Photonics **1**, 97 (2007).
[2]E. Herbst and E. F. van Dishoeck, Annu. Rev. Astron. Astrophys. **47**, 427 (2009).
[3]T. J. Balle and W. H. Flygare, Rev. Sci. Instrum. **52**, 33 (1981).
[4]A. O'Keefe and D. A. G. Deacon, Rev. Sci. Instrum. **59**, 2544 (1988).
[5]G. A. Blake, "Microwave and terahertz spectroscopy," *Encyclopedia of Chemical Physics and Physical Chemistry*, edited by J. H. Moore and N. D. Spencer (Institute of Physics Publishing, Bristol, 2001), Part B1.4, Vol. 2.
[6]S. T. Shipman and B. H. Pate, "New techniques in microwave spectroscopy," *Handbook of High-Resolution Spectroscopy*, edited by M. Quack and F. Merkt (John Wiley & Sons, Ltd., Hoboken, 2011).
[7]E. Gerecht, K. O. Douglass, and D. F. Plusquellic, Opt. Express **19**, 8973 (2011).
[8]G. B. Park, A. H. Steevees, K. Kuyanov-Prozument, J. L. Neill, and R. W. Field, J. Chem. Phys. **135**, 024202 (2011).
[9]A. L. Steber, B. J. Harris, J. L. Neill, and B. H. Pate, J. Mol. Spectrosc. **280**, 3 (2012).
[10]R. Schiwon, G. Schwaab, E. Brundermann, and M. Havenith, Appl. Phys. Lett. **83**, 4119 (2003).
[11]G. W. Schwaab, Proc. SPIE **4111**, 133 (2000).
[12]A. I. Meshkov and F. C. De Lucia, Rev. Sci. Instrum. **76**, 083103 (2005).
[13]R. Braakman and G. A. Blake, J. Appl. Phys. **109**, 063102 (2011).
[14]"Electrical resistivity of pure metals," in *CRC Handbook of Chemistry and Physics*, 93rd ed., edited by W. M. Haynes (CRC Press, Boca Raton, FL, 2013), internet version.
[15]A. E. Costley, K. H. Hursey, G. F. Neill, and J. M. Ward, J. Opt. Soc. Am. **67**, 979 (1977).
[16]I. Yamada, K. Takano, M. Hangyo, M. Saito, and W. Watanabe, Opt. Lett. **34**, 274 (2009).
[17]R. Ulrich, Infrared Phys. **7**, 37 (1967).
[18]P. Goldsmith, *Quasioptical Systems: Gaussian Beam Quasioptical Propagation and Applications* (Wiley, New York, 1998).
[19]Z. Seres, A. Galonsky, K. Ieki, J. J. Kruse, and P. D. Zecher, "Optical transmission of Mylar and Teflon films," Opt. Eng. **33**(9), 3031 (1994).
[20]Y. Gong and B. Li, Proc. SPIE **6720**, 67201E (2007).
[21]J. J. Whalen and C. R. Westgate, Appl. Phys. Lett. **15**, 292 (1969).
[22]D. Halmer, G. von Basum, P. Hering, and M. Mürtz, Rev. Sci. Instrum. **75**, 2187 (2004).
[23]J. C. Laas, B. M. Hays, and S. L. Widicus Weaver, "A multipass millimeter/submillimeter spectrometer to probe dissociative reaction dynamics," J. Phys. Chem. A (in press).

Downloaded 15 Jul 2013 to 170.140.190.145. This article is copyrighted as indicated in the abstract. Reuse of AIP content is subject to the terms at: http://rsi.aip.org/about/rights_and_permissions